Monitoring Interface Interactions by XPS at Nanometric Tin Oxides Supported on Al_2O_3 and Sb_2O_x

Rainer Reiche and Steffen Oswald

Leibniz-Institut für Festkörper-und Werkstoffforschung Dresden, Postfach 270116, 01171 Dresden, Germany

Francisco Yubero, Juan P. Espinós, Juan P. Holgado, and Agustin R. González-Elipe*

Instituto de Ciencia de Materiales de Sevilla (CSIC−University Sevilla) and Dpt. Q. Inorgánica, Avda. Américo Vespucio s/n, E-41092 Sevilla, Spain

Received: November 26, 2003; In Final Form: March 15, 2004

Two model systems consisting of nanometric SnO and SnO_2 particles deposited by evaporation on Al_2O_3 and Sb_2O_3 or Sb_2O_x substrates (x means a mixture of Sb^{3+} and Sb^{5+} oxidation states) are studied by X-ray photoelectron spectroscopy to account for the interactions that develop at the interfaces. The conclusions derived from this study are relevant for the characterization by this technique of nanostructured materials formed by nanoparticles and/or very thin films of an oxide deposited on another oxide support. Electronic parameters such as the binding energy (BE) of the Sn $3d_{5/2}$ photoemission peak and the Auger parameter (α') of the metal cation of the deposited tin oxides shift systematically from a nanometric size of the deposited moieties to a thick layer of these materials. The changes in the electronic parameters between the thickest layers of the deposited oxides and the first deposition situations (i.e., ΔBE, $\Delta\alpha'$, both in eV) are as follows for the different systems: SnO/Al_2O_3 ($\Delta BE = 1.0$, $\Delta\alpha' = -1.6$), SnO/Sb_2O_3 (0.6, −0.7), SnO_2/Al_2O_3 (0.9, −1.2), and SnO_2/Sb_2O_x (0.6, −0.6). These variations are stronger than those existing between Sn^{2+} and Sn^{4+} species in their respective bulk oxides (i.e., approximately 0.5 eV for both ΔBE and $\Delta\alpha'$). These changes are systematized within the concept of the "Chemical state vector" and explained on the basis of a model that considers both the development of specific interactions between the substrates and tin oxide nanoparticles and the influence of different polarizabilities by the surrounding media on the relaxation energy of the photoholes. The changes in the electronic parameters for the initial states of deposition are correlated with the size and shape of the nanoparticles deposited, as determined by XPS peak shape analysis using the Tougaard's method. The analysis of the spectra shows that the tin oxides grow on both substrates in the form of small particles that do not cover completely the substrate before ∼10 Å of material is deposited. It is found that when ∼2 Å of material is deposited, small clusters of approximately ∼8 Å (i.e., about two Sn−O monolayers) cover ∼18% of the surface. Changes in the width of the photoemission peaks are also detected. Removal of surface charging when depositing SnO is responsible for part of these changes, although very likely local inhomogeneities in coordination around the cations also contribute to broadening the peaks. This is particularly important for the smallest nanoparticles where the degree of interface interactions with the substrate is high. Finally, a shift of the valence band edge toward higher binding energies is observed at the initial stages of deposition of tin oxide nanoparticles. This shift is related with particle size effects and/or the development of specific interactions at the interface between the nanoparticles and the support.

Introduction

Metal oxides supported in the form of nanometric particles or very thin films on the surface of other oxides are interesting systems which are used as catalysts, ceramics, sensors, magnetoresistive devices, etc.[1−8] When dealing with this type of nanomaterials, the properties associated with the size of the nanometric particles (or thickness in the case of thin films) of the deposited oxide phase may be affected by two interrelated factors: the changes in electronic structure induced by the particle size and the electronic and/or chemical interactions developing at the interface with the other oxide. In previous publications, we have developed a model to deal with this type of interactions by means of X-ray photoelectron spectroscopy (XPS).[9,10] This experimental technique benefits from the Auger parameter concept, proposed by Wagner,[11] and whose use for the investigations of oxide materials has been systematized by Moretti.[12] Within the aforementioned model, we considered the influence of two types of phenomena, an electronic interaction due to the different chemical nature of the two oxides brought in contact at the interface and a polarization contribution.[10] Many oxide/oxide interfaces have been studied by using these ideas,[9,10,13−16] and the so-called "chemical state vector" (CSV) concept[17] has been proposed to systematize the changes in binding energy (BE) of the photoemission peaks and the Auger parameter (α') of the cations of the nanometric oxide phase. A systematic interpretation of many experimental results available for different oxide/oxide systems can be found in ref 18.

The idea that the BE of photoemission peaks of metal cations depends solely on their oxidation state is widely used in the scientific community using XPS to characterize oxides. Thus,

* Corresponding author. E-mail agustin@cica.es.

10.1021/jp031274m CCC: $27.50
Published on Web 06/10/2004

in many publications dealing with a metal oxide in the form of nanoparticles and/or very thin films supported on the surface of another oxide the possibility that changes in this electronic parameter can be due to the interaction with the oxide support is not considered.[19−21] This may lead to mistakes in the attribution of oxidation states since they are usually defined by the mere comparison with the BE of bulk compounds reported in tables or handbooks. Moreover, shifts in the Auger parameter are not always determined, despite the fact that this parameter bears interesting information about the system properties.

With the present article, we want to get a deeper insight into the interactions occurring at the interface between an oxide substrate and a deposited nanometric oxide. In our previous studies on this type of systems we have mainly paid attention to the shifts in electronic parameters (i.e., BE and α').[18] Here, we have realized that changes due to interface interactions may also affect the width of the peaks and/or to the position of the valence band edge of the nanometric oxide.

For this study we have chosen two model systems consisting of tin oxide, SnO and SnO_2, deposited by evaporation on Al_2O_3, Sb_2O_3, and Sb_2O_x flat surfaces ($x > 3$, indicates that the surface of the antimony oxide is a mixture of Sb^{3+} and Sb^{5+} species). This choice has been firstly supported by the industrial interest of the corresponding real materials (catalysts[22,23] or gas sensors[24]). The study of systems with different physical characteristics such as the SnO and SnO_2 nanoparticles, and the Al_2O_3 and Sb_2O_x substrates have also been considered. Thus, while SnO is a narrow band gap semiconductor that, in practice, can be considered as a metal, SnO_2 is a wide gap semiconductor ($E_{gap} = 3.2$ eV).[25,26] Conversely, Al_2O_3 is an insulator with a relatively low dielectric constant,[27] while Sb_2O_5 and Sb_2O_3 are oxides with electronic structures and dielectric constants similar to those of SnO and SnO_2 (i.e., Sn and Sb are both post transition elements where the "inert" valence s^2 electron pair confer similar properties to their compounds).

Experimental Section

The XPS measurements were done simultaneously on Sb_2O_3 (or Sb_2O_x, see below) and Al_2O_3 single crystals. Sb_2O_3 single crystals were grown by chemical transport in silica ampules as described previously.[28] These single crystals were used as prepared, and no specific effects related to the exposed crystal face was searched. Al_2O_3 was either an optically polished sapphire plate (Goodfellow) or a thin film grown on an aluminum foil. Before deposition of tin oxide, the two oxide substrates were cleaned in situ in the preparation chamber of the XPS spectrometer by bombardment with O_2^+ ions of 3.5 keV kinetic energy and a current density of 10 μA cm^{-2}. This cleaning procedure is fairly effective for removing carbon impurities, and only leads to a mild oxidation of the Sb_2O_3 substrate with the formation of approximately 13% Sb^{5+} species in the surface region.[28] Another cleaning protocol consisted of exposing the oxide samples to an oxygen plasma ($\sim 10^{-2}$ mbar) in the preparation chamber of the spectrometer up to the complete removal of the contaminating carbon. The plasma was produced by a microwave cavity in a quartz tube attached to the preparation chamber. This second procedure was used when the deposited tin oxide was oxidized by plasma to get a SnO_2 stoichiometry. An effect of the oxygen plasma on the Sb_2O_3 substrate is the formation of up to 51% Sb^{5+} species.[28] Under these conditions the substrate surface layers were a mixture of Sb^{3+} and Sb^{5+} species giving an average stoichiometry close to Sb_2O_4. Plasma oxidation was also applied to produce an Al_2O_3 thin film of about 2 nm thickness on an Al foil. This material was used as a substrate to avoid the influence of severe charging effects appearing for SnO_2 deposited on the insulating sapphire plates.[29]

TABLE 1: Preparation Protocols and XPS Spectrometers Used in This Work

system	preparation protocol	XPS spectrometer	X-ray source
SnO/Al_2O_3	O_2^+ bombardment	PHI 5600 CI	Mg Kα
SnO/Sb_2O_3	O_2^+ bombardment	PHI 5600 CI	Al Kα
SnO_2/Al_2O_3	O_2* plasma cleaning	VG-ESCALAB	Mg Kα
SnO_2/Sb_2O_x	O_2* plasma cleaning	VG-ESCALAB	Al Kα

Tin oxide was deposited simultaneously on the two oxide substrates by resistive evaporation from a homemade Knudsen cell filled with SnO powder (Goodfellow). Evaporation was carried out in the preparation chamber of the spectrometer with a base pressure better than 5×10^{-8} mbar. Since the distance from the evaporation cell to the position was relatively high, the amount of tin oxide arriving onto the two substrates was virtually the same.

XPS measurements were carried out with nonmonochromatized Al Kα and Mg Kα excitation sources for the samples deposited on Sb_2O_3 and Al_2O_3 substrates, respectively. The use of two sources was necessary to avoid the overlapping of photoemission and Auger peaks. For the plasma-treated samples, the instrument used was a VG-ESCALAB 210 electron spectrometer working in the constant pass energy mode at a value of 20 eV when recording core level peaks and 50 eV when recording valence band (VB) and Auger spectra. The experiments consisting in the analysis of the deposited tin oxide without any further plasma treatment were conducted in a Physical Electronics PHI 5600 CI electron spectrometer operated in the constant pass energy of 12 eV when recording core level peaks and 24 eV when recording VB and Auger spectra. The energy resolution was similar for the respective peaks at the pass energies chosen for the two instruments.[16] A summary of the different experiments carried out in this paper according to the spectrometer and preparation conditions is presented in Table 1. The BE scale of the two spectrometers was calibrated with a sputter-cleaned copper foil by using the Cu $2p_{3/2}$ (932.7 eV) and Cu 3p (75.15 eV) lines. For the insulating Sb_2O_3 single crystals, referencing of the BE scale was done with respect to the Sb $3d_{3/2}$ peak at 539.95 eV or, for the plasma-exposed samples, at 540.5 eV, in agreement with the peak-fitting analysis of the Sb_2O_3 substrate after ion bombardment and plasma treatments.[16,28] BE referencing of the spectra taken with the Al_2O_3 substrate was done with respect to the Al 2p peak at 75 eV. With these reference values, the Sn photoemission parameters (i.e., Sn $3d_{5/2}$ and α') of a thick film of SnO or SnO_2 compare well with the BE and α' values taken for thick SnO_2 and SnO layers on sputter-cleaned copper[29] or silver.[9] In a previous paper,[29] we found that for insulator plates as substrates, charging effects may influence the value of the Auger parameter. These odd effects were negligible when leaving the samples floating during measurements as was the case in the present work. A maximum error bar of 0.2 eV has been estimated for the determination of α' of the thickest tin oxide overlayers considered here. For the Al_2O_3 substrate, it was found that the Auger parameter of Al changed slightly with the amount of deposited Sb_2O_3. This introduces an uncertainty in the determination of the peak energies but not in that of the Auger parameter that is independent of charge referencing. This uncertainty has been estimated in 0.1 eV. Each deposition of tin oxide will be represented by the Sn/M (M represents Sb or Al) ratio determined from the area of the corresponding Sn $3d_{3/2}$ and Sb $3d_{3/2}$ or Al 2p photoelectron peaks normalized by the

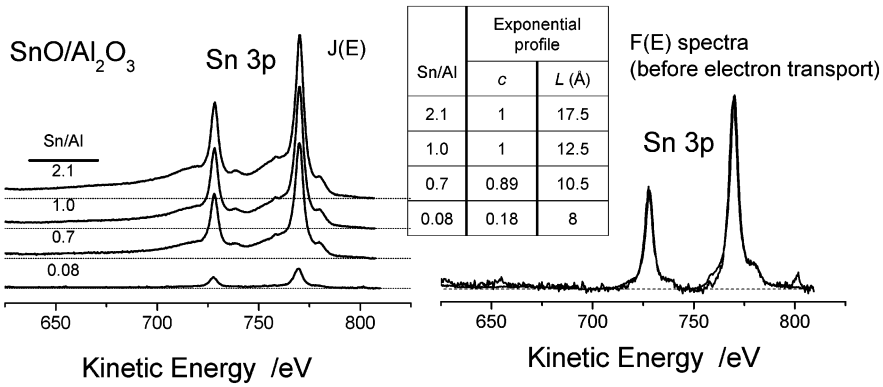

Sn/Al	Exponential profile	
	c	*L* (Å)
2.1	1	17.5
1.0	1	12.5
0.7	0.89	10.5
0.08	0.18	8

Figure 1. Results of the determination of the nanostructure of the deposited SnO on Al_2O_3 by XPS peak shape analysis of the Sn 3p signal. Left: measured J(E) spectra corresponding to Sn/Al ratios of 2.1, 1.0, 0.7, and 0.08. Right: primary excited spectra F(E) before electron transport obtained after QUASES analysis of J(E) peaks. Inset: table with the parameters describing the exponential profile for each case.

corresponding sensitivity factors[30] after a Shirley-type background subtraction. This ratio is a function of both the amount of deposited tin oxide and its degree of dispersion on the surface. Additionally, the Sn/Al ratio is corrected for differences in analyzer transmission[16] and in the inelastic mean free path at the kinetic energies of the photoelectrons involved. For this, the Al 2p intensity was corrected (the Al 2p substrate photoelectrons have the longer inelastic mean free path) by assuming that the ratio O/Al for the sputter-cleaned Al_2O_3 sapphire substrate equaled the stoichiometry ratio 1.5 at the effective information depth of the O 1s photoelectrons, the latter having the same inelastic mean free path as Sb 3d and practically the same as Sn 3d photoelectrons.

Results

The surface morphology of the SnO deposits has been accounted for by applying XPS peak shape analysis (Tougaard method)[31,32] using the QUASES software.[33] This type of analysis relies on a consistent description of the electron transport of the primary excited spectrum F(E) through a given in-depth profile to reproduce measured spectra J(E). For the case of a series of SnO deposits on Al_2O_3, satisfactory analysis for the full series was obtained using an exponential distribution of island heights[34] characterized by the surface coverage *c* and a characteristic length *L*. This means that the deposited tin oxide nanoparticles are characterized by an inhomogeneous distribution of sizes, with *L* the mean height of the particles. We have analyzed the Sn 3p signal coming from the deposited moieties of tin oxide considering an electron inelastic mean free path of 16 Å.[35] Figure 1 shows the measured spectra J(E) for Sn/Al ratios of 0.08, 0.7, 1.0, and 2.1 together with the calculated primary excited spectra F(E) obtained from the analysis. An inset is also included with a table that correlates the Sn/Al ratio with the *c* and *L* parameters of the corresponding in-depth profile. According to this analysis, full coverage (i.e., $c = 1$) is achieved only for Sn/Al $\geq$ 1. For Sn/Al = 0.7, 89% of the surface is covered by the SnO nanoclusters and for Sn/Al = 0.08, only 18% of the surface is covered. In this later case, the height of the clusters is ~8 Å (i.e., about two Sn−O monolayers). The fact that we do not have full coverage in the first stages of growth suggests that nanoparticle growth takes place from the very beginning of deposition. On the other hand, the best analysis is obtained by assuming that the particle height follows an inhomogeneous distribution of island heights. This indicates that there is an inhomogeneous distribution of island heights on the surface of the substrate. The consistency of the XPS peak shape analysis performed is worth noting: nearly identical primary excited spectra F(E) (Figure 1, right) are obtained from the analysis of the different samples J(E) (Figure 1, left).

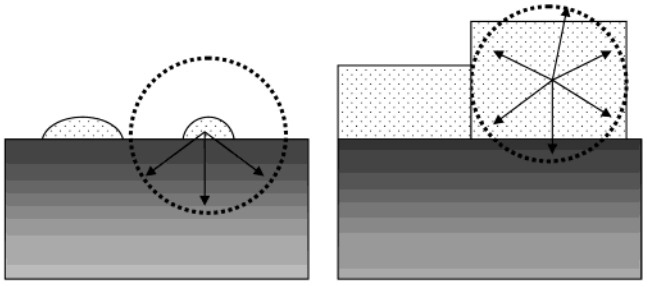

Figure 2. Scheme of polarization effects induced by a photohole in a nanoparticle at different stages of growth, the interface interaction decreases with increasing size of the particle.

Similar results were obtained for the other systems measured here (data not included for simplicity). This means that for low Sn/M ratios (Sn/M < 1) these systems consist of isolated nanoparticles of SnO or SnO_2 of two or more Sn−O monolayer thickness directly interacting with the support. In all cases the XPS peak shape analysis has shown that for higher ratios the size of these particles increases and consequently the degree of interface interaction relatively decreases with the amount of deposited material. The scheme in Figure 2 shows a pictorial description of these ideas for depositions of increasing Sn/M ratio values, with an indication of the different type of contributions from the polarization of the environment of the tin cations in the deposited phase.

BE and Auger Parameter Shifts. Figure 3 shows the Sn 3d photoemission peaks and the Sn MNN Auger peaks for increasing amounts of SnO deposited on Al_2O_3. These spectra show that the position of the peaks shifts systematically with the Sn/Al ratio. Similar effects, although of different magnitude, could be observed for SnO_2 deposited on Al_2O_3 and Sb_2O_x and for SnO on Sb_2O_3. Plots in Figures 4 and 5 summarize the changes observed in the position of the photoelectron peaks (i.e., BEs) and in the value of the Auger parameter (α') for this series of experiments (the Auger parameter α' is defined according to $\alpha' =$ BE (Sn $3d_{5/2}$) + KE (Sn $M_4N_{45}N_{45}$), where KE means kinetic energy of the Auger peak). An advantage of the Auger parameter is that, in principle, it is not sensitive to charging effects on the sample.[11,12,18] However, special care must be given to measurement conditions when investigations of nonconducting material on insulating bulk substrates are carried out.[29] For SnO_2 deposited on Al_2O_3 we used the thin film substrate (cf. Experimental), whereas on Sb_2O_3 single crystals charging

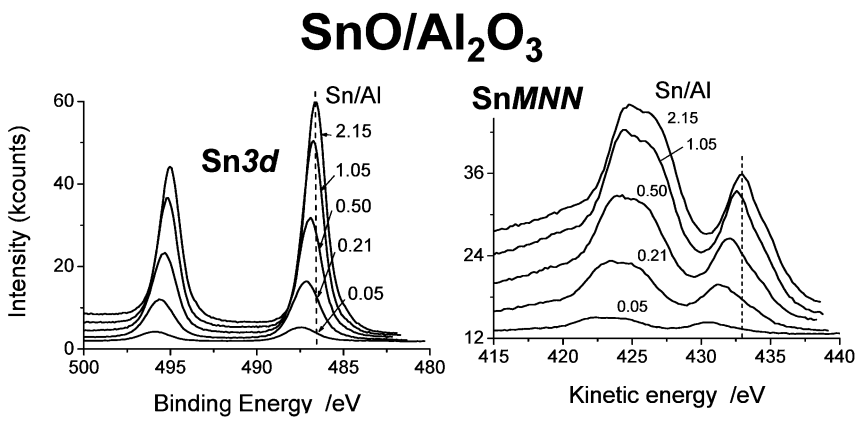

Figure 3. Sn 3d photoemission peaks and Sn MNN Auger peaks for increasing amounts of SnO deposited on Al_2O_3.

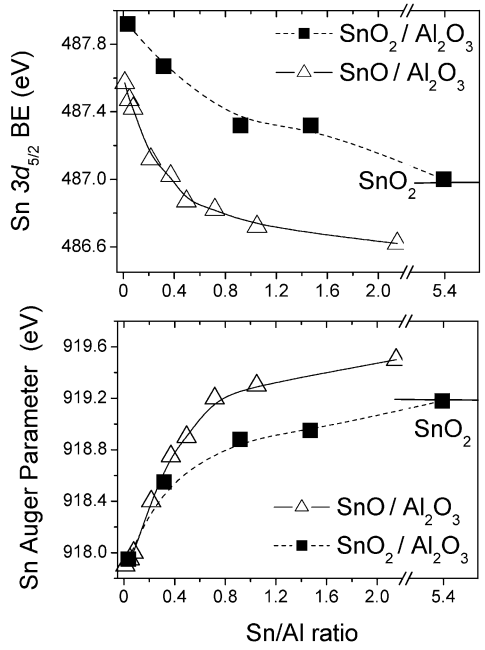

Figure 4. BEs of Sn $3d_{5/2}$ photoemission peaks and Auger parameter values for SnO and SnO_2 deposited on Al_2O_3 as a function of the Sn/Al ratio. The lines are plotted to guide the eye. Also given in the graphs are the values of bulk SnO_2 measured within the same deposition series on metallic copper.[29]

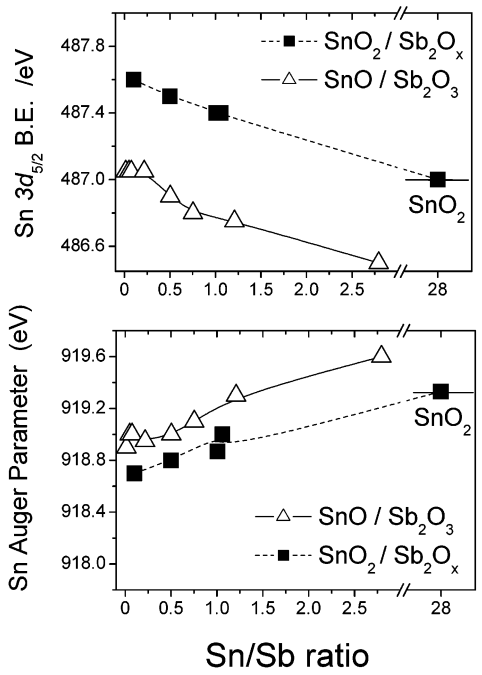

Figure 5. BEs of Sn $3d_{5/2}$ photoemission peaks and Auger parameter values for SnO and SnO_2 deposited on Sb_2O_3 and Sb_2O_x as a function of the Sn/Sb ratio. The lines are plotted to guide the eye. Also given in the graphs are the values of bulk SnO_2 measured within the same deposition series on metallic copper.[29]

artifacts in α′ were avoided by leaving the sample floating without a connection to earth during the measurement. Another possibility would be that a differential charging depending on depth from the surface could influence differently the energies of the Auger and photoemission peaks. However, such an effect should be disregarded here because of the monolayerlike character of the initial deposits and the fact that the thick layers present the value of the bulk tin oxides. Plots are presented for SnO and SnO_2 deposited on Al_2O_3 (Figure 4) and for the two oxides deposited on Sb_2O_3 and Sb_2O_x (Figure 5). As a general trend, these plots show that while the BE decreases with the amount of deposited oxide (expressed as Sn/M atomic ratios), the Auger parameter increases. For both SnO_2 and SnO, the final values are very close to those of bulk SnO[9] or SnO_2 [29] as determined for thick layers of these compounds deposited on metallic substrates. A maximum error bar of 0.1 eV for BEs and less than 0.2 eV for α′ have been estimated for the lowest Sn/M ratios.

Another interesting feature detected when SnO was deposited on Al_2O_3 was the observation of a small shift in the value of the Auger parameter of Al (defined as BE (Al 2p) + KE (Al KLL)), from low to high Sn/Al ratios. As reported in Figure 6 a shift of approximately 0.2 eV is estimated from low to high Sn/Al ratios. Note that the estimated error bar in this case is ∼0.1 eV, smaller than for the deposited SnO owing to the

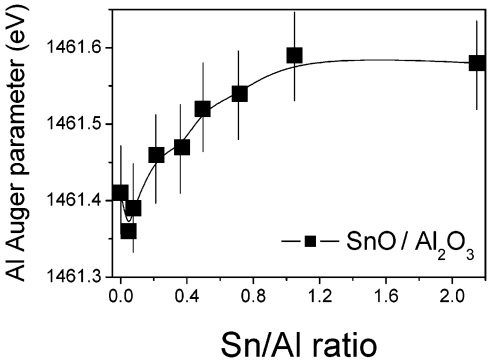

Figure 6. Auger parameter values of Al for SnO deposited on Al_2O_3 as a function of the Sn/Al ratio. The line is plotted to guide the eye.

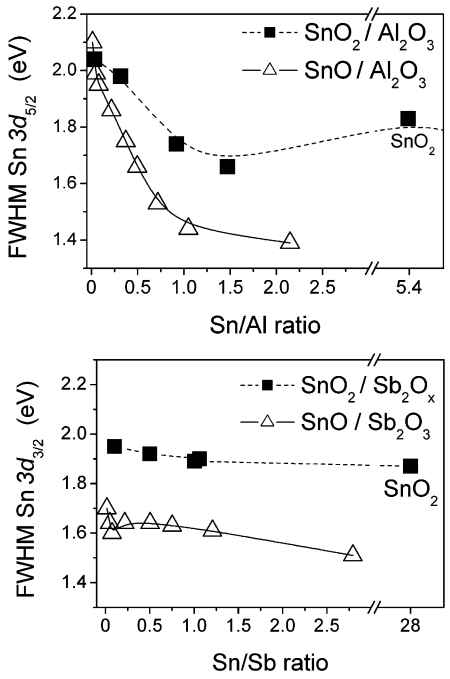

Figure 7. fwhm values of the Sn $3d_{3/2}$ peak for SnO and SnO_2 deposited on Al_2O_3 and Sb_2O_3 or Sb_2O_x as a function of the Sn/M ratios. The lines are plotted to guide the eye. Also given in the graphs is the fwhm value of bulk SnO_2 measured within the same deposition series on metallic copper.[29]

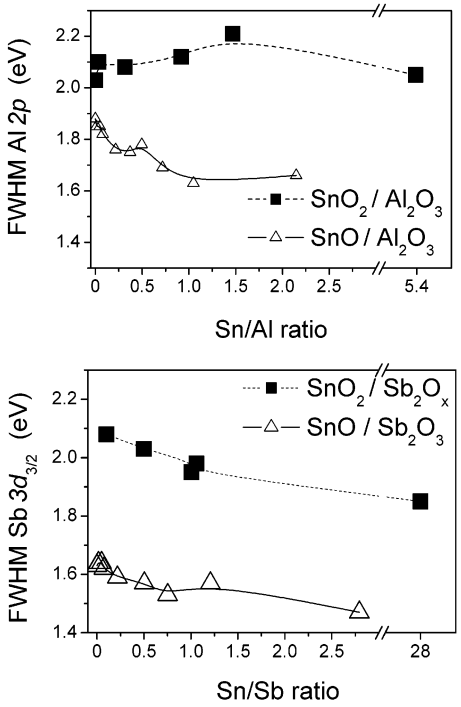

Figure 8. fwhm values of the Al 2p and Sb $3d_{3/2}$ peaks of the substrates for SnO and SnO_2 deposited on Al_2O_3 and Sb_2O_3 or Sb_2O_x as a function of the Sn/M ratios. The lines are plotted to guide the eye.

different intensity of the Sn $3d_{5/2}$ and Al 2p peaks, particularly at low ratios.

Peak Widths. Besides the changes affecting the electronic parameters, we have examined the evolution of the width of the peaks with the Sn/M ratio. It should be noted that peak broadening can be induced by differential changing. These effects can be extremely dependent on the instrument, particularly with insulating materials and/or overlayers (i.e., in this work Al_2O_3 and SnO_2, respectively). Figure 7 shows the values of the full width at half-maximum (fwhm) of the Sn $3d_{3/2}$ peak for SnO and SnO_2 deposited on Al_2O_3 and Sb_2O_3 or Sb_2O_x. For the deposition of SnO or SnO_2 on Al_2O_3, it appears that for low Sn/Al ratios the width of the peaks is similar for the two oxides (i.e., about 2.0 eV), but decreases for high Sn/Al ratios, by 0.3−0.4 eV for SnO_2 and by 0.7 eV for SnO. On antimony oxide, although SnO_2 peaks are wider than those of SnO (for high Sn/Sb ratios the values were 1.9 and 1.5 eV, respectively), the magnitude of Δfwhm as a function of the Sn/Sb ratio is much smaller. The Sn $3d_{3/2}$ peak width changes by only 0.1−0.2 eV for SnO and even less for SnO_2.

In the course of this experiment it was also possible to detect changes affecting the width of the photoemission peaks of the substrate. Usually, changes affecting the width of the photoemission peaks of the substrate in experiments of this kind are not reported. Figure 8 shows the fwhm values for the Al 2p and the Sb $3d_{3/2}$ photoemission peaks as a function of the Sn/M ratio. Al 2p fwhm values of the Al_2O_3 substrate remained almost constant when SnO_2 was the deposited phase, being always larger with this oxide than with SnO. Also interesting is that the Al 2p fwhm values decreased by 0.2−0.3 eV when SnO was the deposited phase. A similar effect was observed with the Sb $3d_{3/2}$ peak, although the maximum Δfwhm was in that case smaller than 0.2 eV. A summary of all these changes is reported in Table 1.

Valence Band Spectra. Valence band (VB) spectra were also recorded as a function of the Sn/M ratio and are presented in Figures 9 and 10 after subtraction of X-ray satellite excitations. The spectra are the superposition of the contributions of the VB spectra of the substrate and the deposited phase. Figure 9 shows a series of VB spectra for SnO deposited on Al_2O_3 and Sb_2O_3, while Figure 10 depicts similar spectra corresponding to SnO_2 deposited on the two substrates. The VB of Al_2O_3 has not much structure and a low photoionization cross section in comparison with the tin oxides;[26,30] therefore, the bands of the deposited phase can be easily identified on Al_2O_3. Deposition of SnO is confirmed at higher Sn/Al ratios by the appearance

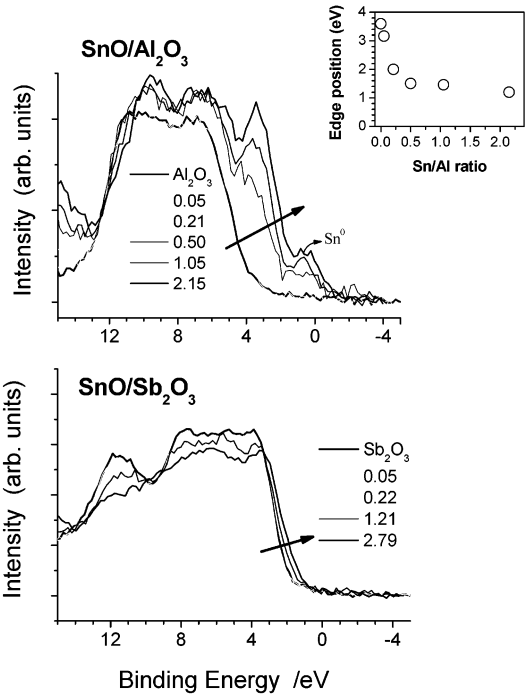

Figure 9. VB spectra for increasing amounts of SnO deposited on Al_2O_3 and Sb_2O_3. The inset summarizes the values of the VB edge positions as a function of the Sn/Al ratios.

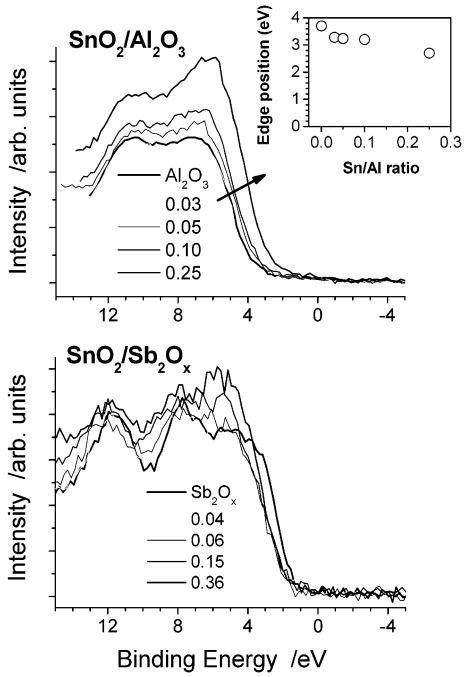

Figure 10. VB spectra for increasing amounts of SnO_2 deposited on Al_2O_3 and Sb_2O_x. The inset summarizes the values of the VB edge positions as a function of the Sn/Al ratios.

of the two characteristic peaks of the Sn $5s^2$ valence distribution at ~3.5 eV and ~9.5 eV and a mainly O 2p-derived peak at around 6−7 eV, although all peaks still shifted by 1 eV to a SnO bulk material.[25,26] For the plasma-exposed samples the typical shape of the SnO_2 VB[26] with the O 2p-derived leading peak at ~5 eV is, apart from the aforementioned 1 eV shift, clearly observed at a low ratio Sn/Al = 0.25. By contrast, the equivalent VB spectrum of SnO deposited on Al_2O_3 for a Sn/Al ratio of 0.21 (cf. Figure 9) only depicts a single leading edge that changes in position with the Sn/Al ratio (see the inset in this figure). In principle, two edges would be expected for a mixture of two noninteracting oxides, one corresponding to the Al_2O_3 substrate and the other to the deposited SnO. Another feature in the spectra is the appearance of a small peak at approximately the origin of the BE scale. This peak is attributed to metallic tin (Sn^0) that sometimes accompanies the deposition of SnO.[9] Since this peak develops only at a high Sn/Al ratio, its influence on the shifts in the VB of the smallest tin oxide particles will be disregarded in the present analysis.

The observed evolution of VB position in the insets of Figures 9 and 10 suggests that the VB edge of the deposited phase shifts with the amount of deposited material. As an additional proof of this effect, we subtracted the VB spectrum of the substrate multiplied by the M/(Sn + M) ratio from that of the experimental spectra. The resulting curves (i.e., actually the contribution of the deposited oxide) edge at BE values similar to those of the experimental spectra. Conversely, when summing the VB spectra of the two bulk oxides multiplied by the M/(Sn + M) and the Sn/(Sn + M) ratios, the position of the experimental edge was not properly reproduced (data not shown). The fact that the magnitude of the overall change for SnO_2 is smaller than that for SnO is due to the semiconductor character of the former making that the band edge of the SnO_2/Al_2O_3 system does not approach so much to the zero of the BE scale even at high Sn/Al ratios. With Sb_2O_3 or Sb_2O_x as substrates, small or negligible effects are observed in the position of the VB edge. The similar VB edge positions of bulk SnO and Sb_2O_3 on one hand (though a small change of 0.8 eV can still be observed), and SnO_2 and Sb_2O_x on the other is the reason why clear shifts are not observed.

Discussion

According to the XPS peak shape analysis (cf. Figure 1), at the initial stages of the deposition experiments our systems can be described as formed by small nanoparticles of an oxide material strongly interacting with another oxide of different nature. In this regard, the systems studied here can be considered as good models for analysis to describe by XPS the interactions developed in nanocomposites formed by small oxide nanoparticles interacting with another oxide acting as support.

The analysis of these model systems by XPS has considered changes in BE and Auger parameters, in the width of photoemission peaks, and in the position of the edge of the valence band (VB) spectra.

BE and Auger Parameter Shifts. In previous articles we have discussed the origin of the BE and α' changes observed when a nanometric oxide, in the form of a very thin film or as nanoparticles, is supported on another oxide. A first step in this analytical procedure consists of representing in a Wagner plot[18] the obtained values for increasing M/M′ ratios. Figure 11 shows the Wagner plots obtained for SnO and SnO_2 deposited on Al_2O_3 and Sb_2O_3 (or Sb_2O_x when working with SnO_2). The points in these plots define a series of "chemical state vectors" (CSV)[17] which are also represented in this figure. The coordinates (i.e., ΔBE, ΔKE) and slope (i.e., ΔKE/ΔBE) of these vectors have been summarized in Table 2. The CSV is defined as vector in a Wagner plot whose origin coincides with the point corresponding to the lowest Sn/M ratio, and its tip with the point representing the bulk material. A CSV defines the whole variation in electronic parameters for a given oxide−oxide system. In that table we have also collected similar parameters taken from a previous work for other SnO, SnO_2/MO systems. This table also reports the variations in the relaxation energy of photoholes at tin sites in the final state (ΔRE) and contributions to the changes in the initial state energy of the systems ($\Delta\epsilon$) between the lowest and the highest Sn/M ratios. This latter deposited state is considered as equivalent to the bulk. The values of ΔRE and $\Delta\epsilon$ are estimated according to the following formulas:

$$\Delta RE = {}^1/_2\Delta\alpha'$$

$$\Delta\epsilon = \Delta RE + \Delta BE$$

According to Table 1, it is apparent that the CSVs have different slopes depending on the substrate. Thus, for SnO deposited on Al_2O_3, the slope was −2.6, while it has a value of −2.1 when SnO was deposited on Sb_2O_3. Similarly, for SnO_2 the slope values were −2.3 when deposited on Al_2O_3 and −2.1 on Sb_2O_x. Slope values equal to −3 indicate that the observed shifts in BE and α' are due exclusively to final state effects of the photoemission process.[12] For systems consisting of small oxide nanoparticles interacting with another oxide, the difference in the relaxation energy of photohole as a function of the Sn/M ratio results from a polarization and a bonding contribution, $\Delta\alpha' = \Delta\alpha'_p + \Delta\alpha'_b$.[18] The first one is a final state contribution due to the different polarizations of the substrate with respect to the deposited phase. This polarization contribution can be approached with the following formula:

$$\Delta\alpha'_p = 11.4/t\,[(1/n_l)^2 - (1/n_s)^2]$$

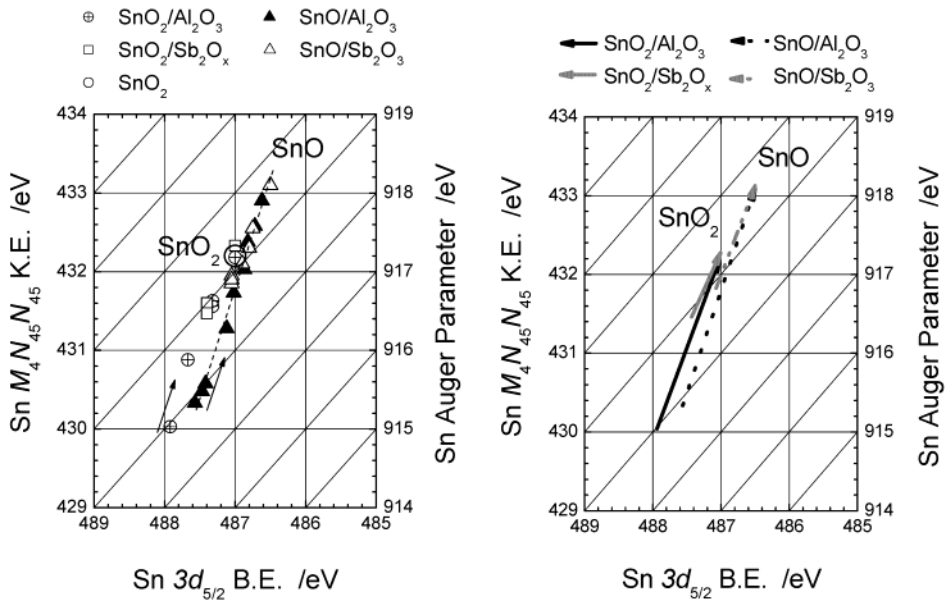

Figure 11. Wagner plot for SnO and SnO_2 deposited on Al_2O_3 and Sb_2O_3 (Sb_2O_x). The CSV of the different systems are indicated in the right-hand panel in this figure.

TABLE 2: Maximum Change in Value of Electronic Parameters of Sn (i.e., coordinates of the tip of the CSV referred to its origin, cf. Figure 11), Full Width at Half Maximum (fwhm) of Photoemission Peaks of Sn, Sb, and Al, and Change in the Auger Parameter of Al, for SnO and SnO_2 Deposited on Al_2O_3 and Sb_2O_3 and Sb_2O_x, Respectively. Slope of CSV and Changes in the Initial ($\Delta\epsilon$) and Final State Energies (ΔRE) Are Also Included (All the energies are in eV.)

system	ΔKE	ΔBE	Δα′	slope	ΔRE	Δϵ	Δfwhm Sn 3d3/2	Δfwhm Al 2p	Δfwhm Sb 3d3/2	Δα′ (Al) Al2O3	ref
SnO/Al_2O_3	−2.6	1.0	−1.6	−2.6	−0.8	0.2	0.7	0.2−0.3	−	0.2	this work
SnO_2/Al_2O_3	−2.1	0.9	−1.2	−2.3	−0.6	0.3	0.3−0.4	0.0	−	−	this work
SnO/Sb_2O_3	−1.3	0.6	−0.7	−2.1	−0.35	0.25	0.2	−	<0.2	−	this work
SnO_2/Sb_2O_x	−1.2	0.6	−0.6	−2.1	−0.3	0.3	0.1	−	0.2	−	this work
SnO/SiO_2	−2.6	0.9	−1.7	−3.0	−0.85	0.0	−				9, 36
SnO_2/SiO_2	−2.8	0.8	−2.0	−3.5	−1.0	−0.2	−				9
SnO/MgO	−2.0	0.5	−1.5	−4.0	−0.75	−0.25	−				9
SnO_2/MgO	−1.8	0.8	−1.0	−2.2	−0.5	0.3	−				9
SnO/C	−0.5	0.2	−0.3	−3.0	−0.15	0.0	−				9, 36
SnO/Ag	1.7	−0.6	1.1	−3.0	0.55	0.0	−				9

where n_l and n_s are the refractive indices of substrate and layer, respectively, and t can be approached as twice the M−O distance in the deposited metal oxide being about 4.5 Å for SnO and 4 Å for SnO_2. Note that n_l^2 and n_s^2 are the dielectric constants of the two materials brought in contact. It can be considered that this expression accounts for the difference in polarization beyond the first coordination sphere when the cation is in a bulk oxide or in small particles and/or thin layers in contact with an oxide of different dielectric constant. According to the scheme in Figure 2, for the small nanoparticles obtained at the initial stages of the deposition experiment, the polarization contribution to the relaxation of photoholes is mainly due to the substrate. By contrast, for the much larger particles formed for high Sn/M ratios, this contribution is mainly due to the tin oxide.

Calculations for the systems studied here ($n_{Al_2O_3} = 1.7$, $n_{SnO_2} = 2.0$, $n_{Sb_2O_3} = 2.2$, $n_{SnO} \gg 10$) and those reported in the literature ($n_{SiO_2} = 1.5$, $n_{MgO} = 1.8$) yield the values reported in Table 2 where we have also summarized the bonding contribution of the first neighbor atoms to the relaxation of photoholes. This second contribution to $\Delta\alpha'$ is determined according to: $\Delta\alpha'_b = \Delta\alpha' - \Delta\alpha'_p$.

An analysis of the results for the different systems whose electronic parameters are summarized in Tables 1 and 2 reveals that the calculated $|\Delta\alpha'_p|$ values for SnO vary according to $SiO_2 > Al_2O_3 > MgO > Sb_2O_3$, i.e., an opposite tendency to that defined by the value of the dielectric constants of the support materials. Meanwhile, the bonding contribution to $\Delta\alpha'$ shows a different behavior ($|\Delta\alpha'_b|$: $Sb_2O_3 < SiO_2 < Al_2O_3 = MgO$). On the other hand, for SnO_2, both $|\Delta\alpha'_p|$ and $|\Delta\alpha'_b|$ decrease in an opposite way than the values of the dielectric constant of the substrate (i.e., $SiO_2 > Al_2O_3 > MgO > Sb_2O_3$). The tendency in the polarization contribution found for both SnO and SnO_2 clearly confirms that the value of $\Delta\alpha'$ is determined by the difference in the dielectric constants of the substrate and the supported oxide. According to the dipolar model of Moretti,[12] $\Delta\alpha'_b$ can be taken as proportional to the polarizability of the first neighbor atoms around the cations (i.e., contribution of the Sn−O bonds to the relaxation energy of the photohole at the Sn atoms). This would indicate that for SnO_2 deposited on the different substrates, the polarizability of the oxide ions around the cations of the first layer in contact with the substrate follows the same trend than the dielectric constants of the substrate materials. However, the different behavior found for SnO poses the question of what is the polarizability of the neighboring oxide ions of the first layer in contact with the substrate.

Assuming a similar local coordination local structure for the cations of this first layer irrespective of the substrate, the tendency in $|\Delta\alpha'_b|$ found for SnO would indicate that the polarizabilities of the first coordination oxide ions change in a

way opposite to the dielectric constant of the substrate. The bonding characteristics of the Sn−O−M structures at the interface and, in particular, the role of the $5s^2$ electrons at tin should be considered to account for this tendency.

Table 1 also shows that for the systems studied here there is a certain variation in the initial state energy (i.e., $\Delta\epsilon$). This difference must be associated with the fact that Sn^{n+} ions (n, formal charge equal to 2 or 4) at the interface have a different density of charge and/or experience a different Madelung potential. Very likely, the formation of Sn−O−M cross linking bonds at the interface, distortions of the local geometries and/or changes in coordination number around the Sn^{n+} ions at the interface are some of the factors provoking the observed changes in ϵ. In this context, it is interesting to recall that in previous photoemission experiments with nanometric SnO deposited on three substrates (Ag, C, SiO_2)[9,36] there were practically no initial state changes. Moreover, on HOPG (i.e., the C substrate) even the relaxation changes were very small and no size effects were detected in the photoemission parameters at very low Sn/C ratios.

Another interesting result from the previous experiments with the SnO/Al_2O_3 system that has not been previously reported for any substrate is the slight change in the Auger parameter detected for the Al 2p peaks (cf. Figure 6). The observed shift, although being close to the uncertainty limit of the measurement, reveals that the interactions developing at the interface also affect the substrate, although its magnitude is small because of its bulk character. This observation introduces an additional source of uncertainty in the experimental evolution of BE values of the overlayer (the measured α' values will not be affected by the actual BE reference used to calibrate the spectra). From the observations in Table 1, where in all cases ΔBE of the overlayer is approximately 0.6−0.7 times the magnitude of $\Delta\alpha'$, we can assume a change in the Al 2p BE of approximately 0.1 eV, from the bare substrate to the fully covered situation. This will be an intrinsic uncertainty contribution to be added to the experimental errors induced by referencing the BE of the nanoparticles to the peaks of the substrate.

Peak Width. The previous results have shown that the fwhm of the peaks of the deposited phase decreases as the Sn/M ratio increases. This narrowing can be due to different factors. A first one is that for the lowest Sn/M ratios, where a high number of tin cations will be interacting with the substrate possibly via Sn−O−M cross linking bonds, the local geometries around the tin ions will be rather heterogeneous. Therefore, the different cations will produce photoemitted electrons with slightly different KEs that will widen the experimental photoemission peak. As the Sn/M ratio increases, the local environments around the Sn ions become more bulklike, while the contribution of the ions at the interface attenuates because of the shadowing by utmost layers of bigger nanoparticles or thicker films. For nonconducting substrates such as Al_2O_3 or Sb_2O_3, a decrease in the differential surface charging when SnO (a conducting material) is deposited on their surface may be another factor contributing to the narrowing of the peaks.[37] The experimental charge shift detected in our case varied from 4.5 eV for the bare Al_2O_3 substrate to 1.2 eV for a relatively thick layer of SnO deposited on it.

The data reported in Figures 7 and 8 and Table 1 show that not only the widths of photoemission peaks of the deposited nanoparticles vary with coverage but, in some cases, also the fwhm of photoemission peaks of the substrate. We believe that the continuous decrease in fwhm of the Al 2p peak for the SnO/Al_2O_3 system is due to the removal of charge broadening effects by the deposition of SnO.

TABLE 3: Polarization and Bonding Interaction Contributions to the Change in the Sn Auger Parameter $\Delta\alpha'$ for the Different SnO_x/MO Systems (All the values are in eV.)

system	$\Delta\alpha'_p$	$\Delta\alpha'_b$
SnO/Al_2O_3	−0.87	−0.73
SnO_2/Al_2O_3	−0.27	−0.93
SnO/Sb_2O_3	−0.52	−0.18
SnO_2/Sb_2O_x	+0.12	−0.72
SnO/SiO_2	−1.12	−0.58
SnO_2/SiO_2	−0.54	−1.46
SnO/MgO	−0.78	−0.72
SnO_2/MgO	−0.15	−0.85

Valence Band Edge. The analysis of the valence band edge of the SnO/MO systems as a function of the Sn/M ratio reveals a "blue shift" (widening of band gap) in the edge of the density of states of the smallest SnO nanoparticles. This shift is particularly noticeable for SnO deposited on Al_2O_3 (cf. Figure 9). In this case, the difference in the band edge positions of bulk Al_2O_3 and SnO enables a clear visualization of the shift of the VB of this latter when it is in the form of supported nanoparticles. Similar observations have been reported for other MO/M′O systems such as TiO_2/SiO_2, Al_2O_3/SiO_2, or Sb_2O_3/Al_2O_3.[10,13,16] A quantum size effect associated to the nanometric size of the deposited particles,[38] the amorphous character of the overlayer or the interaction of the nanometric particles with the substrate are claimed as possible reasons for the observed shift. In a previous publication on the TiO_2/SiO_2 interface,[10] we were able to simulate by quantum mechanical calculations that the interaction with a substrate with a higher insulating character contributes to widening the band gap of the supported nanometric phase. The results obtained here for the SnO nanoparticles deposited on Al_2O_3 show that they tend to approach the insulating character of this latter when the size of the particles is small and they strongly interact with the substrate. Similar metal-to-insulator transitions have been reported for deposited metal particles as a function of their size.[39]

Concluding Remarks

The routine use of XPS to determine the oxidation state of elements in materials, including composite nanomaterials, rely on the measurement of the BE position of photoemission peaks. We have shown that this parameter can vary as an effect of the interaction of the nanoparticles with another material acting as substrate or as a matrix host. The magnitude of these changes can be as large or even larger than those expected for different oxidation states of a cation in different bulk compounds. The case of tin oxide is paradigmatic in this respect. In fact, ΔBE of Sn $3d_{5/2}$ peaks between bulk SnO and SnO_2 amounts to ∼0.5 eV, while the variations in this parameter due to the interaction of SnO or SnO_2 nanoparticles with a substrate such as Al_2O_3 is 1.0 and 0.9 eV, respectively.

These examples support the need of using another parameter such as the Auger parameter to characterize oxide nanoparticles in composite systems. We have shown that the systematic analysis of the changes of this parameter and the systematization of the results within the CSV concept open useful ways of addressing the problem of the electronic and polarization interactions developing at the interface between two oxide materials, one of them of nanometric size (Table 3).

Acknowledgment. This work has been carried out within the framework of a German-Spanish "Accion Integrada"

cooperation action. The Sb_2O_3 single crystal substrates were kindly supplied by Dr. Behr and his team at the IFW Dresden. We also thank the Spanish Ministry of Science and Technology (Projects MAT2000-1505-C02-01 and MAT2001-2820) and the Deutsche Forschungsgemeinschaft (DFG, project WE 1519/10) for financial support.

References and Notes

(1) *Surfaces and Interfaces of Ceramic Materials*; Dufour, L. C., Monty, C., Petot-Ervas, G., Eds.; Kluwer Academic: Dordrecht, 1989.

(2) *Science of Ceramic Interfaces*; Nowotny, J., Ed.; Elsevier: Amsterdam, 1991.

(3) Prins, R.; de Beer, V. H. J.; Somorjai, G. *Catal. Rev. Sci. Eng.* **1989**, *31*, 1.

(4) Brun, N.; Colliex, Ch.; Rivory, J.; Yu-Zhang, K. *Microsc. Microanal. Microstruct.* **1998**, *7*, 1.

(5) Ovenston, A.; Sprinceana, D.; Walls, J. R.; Caldararu, M. *J. Mater. Sci.* **1994**, *29*, 4946.

(6) Li, C.; Wang, J.; Su, W.; Chen, H.; Wang, W.; Zhuang, D. *Physica B* **2001**, *307*, 1.

(7) Mittov, O. N.; Ponomareva, N. I.; Mittova, I. Y. *Inorg. Mater.* **2002**, *38*, 576.

(8) Szczuko, D.; Werner, J.; Behr, G.; Oswald, S.; Wetzig, K. *Surf. Interface Anal.* **2001**, *31*, 484.

(9) Jiménez, V. M.; Espinós, J. P.; González-Elipe, A. R. *Surf. Sci.* **1996**, *366*, 556.

(10) Mejías, J. A.; Jiménez, V. M.; Lassaletta, G.; Fernández, A.; Espinós, J. P.; González-Elipe, A. R. *J. Phys. Chem.* **1996**, *100*, 16255.

(11) Wagner, C. D.; Joshi, A. *J. Electron. Spectrosc. Relat. Phenom.* **1988**, *47*, 283.

(12) Moretti, G. *J. Electron. Spectrosc. Relat. Phenom.* **1998**, *95*, 95.

(13) Reiche, R.; Yubero, F.; Espinós, J. P.; González-Elipe, A. R. *Surf. Sci.* **2000**, *457*, 199.

(14) Espinós, J. P.; Morales, J.; Barranco, A.; Caballero, A.; Holgado, J. P.; González-Elipe, A. R. *J. Phys. Chem. B* **2002**, *106*, 6921.

(15) Barranco, A.; Yubero, F.; Mejías, J. A.; Espinós, J. P.; González-Elipe, A. R. *Surf. Sci.* **2001**, *482/485*, 680.

(16) Reiche, R.; Dobler, D.; Holgado, J. P.; Barranco, A.; Martín-Concepción, A.; Yubero, F.; Espinós, J. P.; González-Elipe, A. R. *Surf. Sci.* **2003**, *537*, 228.

(17) Barranco, A.; Yubero, F.; Espinós, J. P.; González-Elipe, A. R. *Surf. Interface Anal.* **2001**, *31*, 761.

(18) González-Elipe, A. R.; Yubero, F. Spectroscopic Characterization of oxide/oxide interfaces. In *Handbook of Surfaces and Interfaces of Materials*; Nalva, H. S., Ed.; Academic Press: San Diego, 2001; Vol. 2, p 147.

(19) Xu, C.; Oh, W. S.; Guo, Q.; Goodman, D. W. *J. Vac. Sci. Technol. A* **1996**, *14*, 1395.

(20) Ruby, C.; Fusa, J.; Génin, J. M. R. *Thin Solid Films* **1999**, *352*, 22.

(21) Biener, J.; Bäumer, M.; Madix, R. J.; Liu, P.; Nelson, E.; Kendelewisz, T.; Brown, G., Jr. *Surf. Sci.* **2000**, *449*, 50.

(22) Sun, K.; Liu, J.; Browing, N. D. *J. Catal.* **2002**, *205*, 266.

(23) Pillep, B.; Behrens, P.; Schubert, U. A.; Splenger, J.; Knözinger, H. *J. Phys. Chem. B* **1999**, *103*, 9595.

(24) Göpel, W.; Schierbaum, K. D. *Sensors Actuators B* **1995**, *26*−*27*, 1.

(25) Jiménez, V. M.; Lassaletta, G.; Fernández, A.; Espinós, J. P.; Yubero, F.; González- Elipe, A. R.; Soriano, L.; Sanz, J. M.; Papaconstantopoulos, D. A. *Phys. Rev. B* **1999**, *60*, 11171.

(26) Themlin, J. M.; ChTaïb, M.; Henrard, L.; Lambin, P.; Darville, J.; Gilles, J. M. *Phys. Rev. B* **1992**, *46*, 2460.

(27) *Handbook of Chemistry and Physics*, 54*th* ed.; CRC Press: Cleveland, 1997; p 363.

(28) Reiche, R.; Holgado, J. P.; Yubero, F.; Espinós, J. P.; González-Elipe, A. R. *Surf. Interface Anal.* **2003**, *35*, 256.

(29) Oswald, S.; González-Elipe, A. R.; Reiche, R.; Espinós, J. P.; Martín, A. *Surf. Interface Anal.* **2003**, *35*, 991.

(30) Yeh, J. J.; Lindau, I. *Atomic Data and Nuclear Data Tables* **1985**, *32*, 1.

(31) Tougaard, S. *J. Vac. Sci. Technol. A* **1996**, *14*, 1415.

(32) Tougaard, S. *Surf. Interface Anal.* **1998**, *26*, 249.

(33) Tougaard, S. *QUASES, Software package for quantitative XPS/AES of surface nanostructures by inelastic peak shape analysis*; see www.QUASES.com.

(34) Yubero, F.; González-Elipe, A. R.; Tougaard, S. *Surf. Sci.* **2000**, *457*, 24.

(35) Tanuma, S.; Powell, C. J.; Penn, D. R. *Surf. Interface Anal.* **1991**, *17*, 927.

(36) Jiménez, V. M.; Fernández, A.; Espinós, J. P.; González-Elipe, A. R. *Surf. Sci.* **1996**, *350*, 123.

(37) Cazaux, J. *J. Electron. Spectrosc. Relat. Phenom.* **1999**, *105*, 155.

(38) Kavan, L.; Stoto, T.; Grätzel, M.; Fitzmaurice, D.; Shklover, V. *J. Phys. Chem.* **1993**, *97*, 9493.

(39) Aiyer, H. N.; Vijayakrishnan, V.; Subbanna, G. N.; Rao, C. N. R. *Surf. Sci.* **1994**, *313*, 392.